



# Measurements of the branching fraction ratio $\mathcal{B}(\phi \rightarrow \mu^+ \mu^-) / \mathcal{B}(\phi \rightarrow e^+ e^-)$ with charm meson decays

LHCb collaboration<sup>†</sup>

## Abstract

Measurements of the branching fraction ratio  $\mathcal{B}(\phi \rightarrow \mu^+ \mu^-) / \mathcal{B}(\phi \rightarrow e^+ e^-)$  with  $D_s^+ \rightarrow \pi^+ \phi$  and  $D^+ \rightarrow \pi^+ \phi$  decays, denoted  $R_{\phi\pi}^s$  and  $R_{\phi\pi}^d$ , are presented. The analysis is performed using a dataset corresponding to an integrated luminosity of  $5.4 \text{ fb}^{-1}$  of  $pp$  collision data collected with the LHCb experiment. The branching fractions are normalised with respect to the  $B^+ \rightarrow K^+ J/\psi(\rightarrow e^+ e^-)$  and  $B^+ \rightarrow K^+ J/\psi(\rightarrow \mu^+ \mu^-)$  decay modes. The combination of the results yields

$$R_{\phi\pi} = 1.022 \pm 0.012 (\text{stat}) \pm 0.048 (\text{syst}).$$

The result is compatible with previous measurements of the  $\phi \rightarrow \ell^+ \ell^-$  branching fractions and predictions based on the Standard Model.

Submitted to JHEP

© 2024 CERN for the benefit of the LHCb collaboration. CC BY 4.0 licence.

<sup>†</sup>Authors are listed at the end of this paper.



# 1 Introduction

A particularly sensitive way of searching for physics beyond the Standard Model (SM) is to make high-precision experimental tests of accidental symmetries that arise in the SM. One such accidental symmetry is lepton flavour universality (LFU), whereby the strength of the electroweak couplings for charged leptons is independent of their flavour. The violation of LFU is a common feature in extensions of the SM, and branching fraction ratios of hadron decays involving different lepton species constitute a sensitive probe for physics beyond the SM, since they are largely free from hadronic uncertainties.

There has been much activity in testing LFU in  $b$ -hadron decays over the last decade at LHCb. In  $b \rightarrow s\ell^+\ell^-$  decays, where  $\ell$  represents either an electron or a muon, the most recent LFU measurements [1, 2] are consistent with the SM with a precision of 5% that is statistically limited. Several cross-checks are performed in the  $b \rightarrow s\ell^+\ell^-$  LFU analyses to reinforce confidence in the results. The most stringent of these checks is the ratio  $r_{J/\psi} = \mathcal{B}(B^+ \rightarrow H_s J/\psi(\rightarrow \mu^+\mu^-))/\mathcal{B}(B^+ \rightarrow H_s J/\psi(\rightarrow e^+e^-))$ , where  $H_s$  represents a strange meson. The measurement of the ratio  $r_{J/\psi}$  requires significantly more control over the efficiencies than the LFU measurements themselves and was found to be compatible with the SM prediction in all measurements [3–7]. The variation of the efficiency as a function of several kinematic variables, such as the maximum transverse momentum of the two leptons, is also performed and no significant systematic effects are seen. Finally, the double ratio for the  $\psi(2S)$  and  $J/\psi$  resonances,  $R_{\psi(2S)}$ , is performed and is also found to be compatible with unity for all measurements [3–7]. The robustness of the efficiency for the existing LFU measurements at the current level of precision is therefore clear. However, as the statistical precision improves in the future, analysing a control channel in the  $q^2$  region complementary to those performed in the existing analyses will be important to keep systematic uncertainties subdominant.

The branching fraction ratios

$$R_{\phi\pi}^{(d,s)} \equiv \frac{\mathcal{B}(D_{(s)}^+ \rightarrow \pi^+\phi(\rightarrow \mu^+\mu^-))}{\mathcal{B}(D_{(s)}^+ \rightarrow \pi^+\phi(\rightarrow e^+e^-))}, \quad (1)$$

where  $\phi$  refers to the  $\phi(1020)$  meson, are ideal quantities in this respect [8]. As the decay is dominated by photon exchange, LFU is expected to hold in this process. The invariant mass of the  $\phi$  meson means that this decay occurs at a  $q^2$  value below many of the existing LFU measurements. The decays  $D_{(s)}^+ \rightarrow \pi^+\phi$  have a large branching fraction [9] and a fully charged final state, meaning that high precision tests can be performed.<sup>1</sup> Furthermore, the current precision of  $\mathcal{B}(\phi \rightarrow \mu^+\mu^-)/\mathcal{B}(\phi \rightarrow e^+e^-)$  is 6%, obtained by comparing the individual branching fraction measurements from Refs. [10–12]. This test is entirely limited by the branching fraction of  $\mathcal{B}(\phi \rightarrow \mu^+\mu^-)$  [12], which provides the opportunity to improve the precision of that branching fraction.

This paper presents a measurement of  $\mathcal{B}(\phi \rightarrow \mu^+\mu^-)/\mathcal{B}(\phi \rightarrow e^+e^-)$  based on a dataset corresponding to an integrated luminosity of  $5.4 \text{ fb}^{-1}$  of  $pp$  collisions collected with the LHCb detector between 2016 and 2018. Similarly to the  $b \rightarrow s\ell^+\ell^-$  LFU measurements performed by the LHCb collaboration, the signals are measured with respect to the  $B^+ \rightarrow K^+ J/\psi(\rightarrow \ell^+\ell^-)$  decay modes. The double ratio strategy, which consists in comparing the branching fraction ratios of signal and normalisation modes

---

<sup>1</sup>The inclusion of the charge-conjugate mode is implied.

with the same topology, ensures that the knowledge of absolute efficiencies is unnecessary. This normalisation assumes that LFU holds in  $J/\psi$  decays, which has been verified well beyond the precision of this measurement [9].

The paper is organised as follows: firstly, a brief overview of the LHCb experiment is given in Sect. 2, along with a description of the dataset. Secondly, the signal selection is given in Sect. 3 and the remaining backgrounds and signal-yield determination are discussed in Sect. 4. The determination of the reconstruction and selection efficiency of the signal and normalisation modes is presented in Sect. 5. The values of these efficiencies were kept blind until the analysis was finalised to avoid experimenter bias. Sources of systematic uncertainties and their impact are discussed in Sect. 6. Finally, the results and conclusion are presented in Sect. 7.

## 2 The LHCb detector and simulation

The LHCb detector [13, 14] is a single-arm forward spectrometer covering the pseudorapidity range  $2 < \eta < 5$ , designed for the study of particles containing  $b$  or  $c$  quarks. The detector includes a high-precision tracking system consisting of a silicon-strip vertex detector surrounding the  $pp$  interaction region [15], a large-area silicon-strip detector located upstream of a dipole magnet with a bending power of about 4 Tm, and three stations of silicon-strip detectors and straw drift tubes [16] placed downstream of the magnet. The tracking system provides a measurement of the momentum,  $p$ , of charged particles with a relative uncertainty that varies from 0.5% at low momentum to 1.0% at 200 GeV/ $c$ . The minimum distance of a track to a primary  $pp$  collision vertex (PV), the impact parameter (IP), is measured with a resolution of  $(15 + 29/p_T) \mu\text{m}$ , where  $p_T$  is the component of the momentum transverse to the beam, in GeV/ $c$ . Different types of charged hadrons are distinguished using information from two ring-imaging Cherenkov detectors [17]. Photons, electrons and hadrons are identified by a calorimeter system consisting of scintillating-pad (SPD) and preshower detectors, an electromagnetic and a hadronic calorimeter. Muons are identified by a system composed of alternating layers of iron and multiwire proportional chambers [18].

Simulation is required to model the effects of the detector acceptance and to account for the imposed selection requirements. In the simulation,  $pp$  collisions are generated using PYTHIA [19] with a specific LHCb configuration [20]. Decays of unstable particles are described by EVTGEN [21], in which final-state radiation is generated using PHOTOS [22]. The interaction of the generated particles with the detector, and its response, are implemented using the GEANT4 toolkit [23], as described in Ref. [24].

## 3 Candidate selection

The online event selection is performed by a trigger [25], which consists of a hardware stage, based on information from the calorimeter and muon systems, followed by a software stage, which applies a full event reconstruction. At the hardware trigger stage, candidates with muons are required to have at least one high- $p_T$  muon track. Decays involving electrons are required to either include a high- $p_T$  electron, a high- $p_T$  hadron or be triggered independently of the final state. The data selected by these three trigger methods in the electron channel are treated as separate categories in the analysis.

The software trigger is split into two stages, with the first requiring one or two tracks with high IP and  $p_T$ . In between the two software stages, an alignment and calibration of the detector is performed in near real-time and the results are used in the second stage of the software trigger [26]. The same alignment and calibration information is propagated to the offline reconstruction, ensuring that the particle identification (PID) is of high quality and consistent between the trigger and offline analysis. The identical performance of the online and offline reconstruction enables physics analyses to be performed directly using candidates reconstructed in the trigger [25, 27], which the present analysis exploits for the signal channels.

In the second software stage, exclusive selection requirements designed to select  $D_{(s)}^+ \rightarrow h^+\ell^+\ell^-$  candidates are applied. Three tracks are required to be inconsistent with originating from any PV, to have  $p_T > 300 \text{ MeV}/c$  and  $p > 2000 \text{ MeV}/c$ . These tracks are combined to form a good-quality vertex that is significantly displaced with respect to any PV. For each electron track, a search is therefore made in the ECAL for bremsstrahlung energy deposits around the extrapolated track direction before the magnet that are not associated with any other charged tracks. The energy of any such deposit is added to the electron energy that is derived from the measurements made in the tracking system. Bremsstrahlung photons can be added to none, either, or both of the final-state  $e^+$  and  $e^-$  candidates. The invariant mass of the reconstructed final state particles is required to fall within  $200 \text{ MeV}/c^2$  of the known  $D^+$  mass [9]. The angle between the momentum vector of the charm meson candidate and the line connecting the PV to the decay vertex must be less than  $14 \text{ mrad}$ . To select the  $\phi \rightarrow \ell^+\ell^-$  decay, a dilepton mass window of  $990 - 1050 \text{ MeV}/c^2$  for muons and  $870 - 1110 \text{ MeV}/c^2$  for electrons is applied.

The trigger strategy for the normalisation mode  $B^+ \rightarrow K^+ J/\psi$  is an inclusive selection that forms two- and three-track combinations with a high-quality vertex that is significantly displaced from any PV. The  $B^+ \rightarrow K^+ J/\psi$  candidates are then built offline, requiring that a well-identified kaon is combined with two leptons to form a high-quality vertex. These candidates must be consistent with originating from a PV and their decay vertex must be significantly displaced from that PV. In order to select the  $J/\psi$  resonance, the dilepton invariant mass is required to be between  $2946 - 3176 \text{ MeV}/c^2$  for muons and  $2450 - 3600 \text{ MeV}/c^2$  for electrons.

The offline selection encompasses invariant mass vetoes and multivariate analysis techniques. Doubly misidentified background from  $D^+ \rightarrow K^-\pi^+\pi^+$  decays, where a kaon and a pion are reconstructed as electrons, is rejected by removing candidates that have a  $K^-\pi^+\pi^+$  invariant mass within  $30 \text{ MeV}/c^2$  of the  $D^+$  mass [9]. Background sources coming from doubly misidentified  $D_{(s)}^+ \rightarrow \pi^+\pi^-\pi^+$  decays with two pions misidentified as electrons are reduced by the use of particle-identification (PID) criteria. The remaining contamination from this source is included in the fit used to determine the signal yield as described in Sect. 4. A kinematic fit that constrains the dilepton invariant mass to the known  $\phi$  ( $J/\psi$ ) mass [9] is performed to each candidate of the signal (normalisation) mode. In the following, these quantities are referred to as  $m_\phi(\pi^+\ell^+\ell^-)$  and  $m_{J/\psi}(K^+\ell^+\ell^-)$ , respectively. Their distributions are used to extract the signal and normalisation yields via maximum-likelihood fits to the data and to define the sideband regions, summarised in Table 1. The dominant source of background is combinatorial in nature, whereby the tracks do not originate from a common particle decay. To reduce this background for both signal and normalisation modes, separate Boosted Decision Tree (BDT) classifiers [28, 29] are trained. The BDT classifiers use a combination of kinematic and geometric information

Table 1: Signal ( $D_{(s)}^+ \rightarrow \pi^+\phi$ ) and normalisation ( $B^+ \rightarrow K^+J/\psi(\rightarrow \ell^+\ell^-)$ ) mode sideband mass ranges. The variables  $m_\phi(\pi^+\ell^+\ell^-)$  and  $m_{J/\psi}(K^+\ell^+\ell^-)$  are used for signal and normalisation decays, respectively.

Decay mode	$m_\phi(\pi^+\ell^+\ell^-)$ [MeV/c <sup>2</sup> ]	$m_{J/\psi}(K^+\ell^+\ell^-)$ [MeV/c <sup>2</sup> ]
$e^+e^-$	$\notin$ [1810,2040]	$> 5580$
$\mu^+\mu^-$	$\notin$ [1840,2000]	$> 5480$

such as the final state impact parameters and kinematics. The most discriminating variable for both signal and normalisation modes is the angle between the momentum vector of the  $D_{(s)}^+$  or  $B^+$  and the line connecting the PV with their decay vertices.

The requirement on the response of the BDT classifier for the signal mode is optimised using the Punzi figure of merit [30]  $N_s/(\sigma/2 + \sqrt{N_b})$ , where  $\sigma = 5$ ,  $N_s$  is the number of signal candidates as determined from simulation, and  $N_b$  is the number of background events extrapolated from the sideband regions for the signal modes. The efficiency for the BDT classifier selection is 59.2% (70.8%) on the electron (muon) signal with a 92.8% (85.4%) rejection rate for the electron (muon) background. To optimise the BDT classifier response in normalisation mode decays, the metric  $N_s/\sqrt{N_b}$  is used instead. The use of this metric results in a very pure sample, which simplifies kinematic comparisons between data and simulation. The signal selection efficiency in this case is 99.2% (92.3%) on the electron (muon) signal, with a 81.5% (87.0%) rejection rate for the electron (muon) background.

## 4 Signal yield determination

The signal yield is determined in categories of the different run periods and trigger conditions by means of a maximum-likelihood fit to the  $m_\phi(\pi^+\ell^+\ell^-)$  distributions of the signal candidates. The  $\phi$  mass constraint significantly improves the invariant-mass resolution in the electron channels and leaves the muon channels largely unchanged. The result of the fit is shown in Fig. 1.

The signal lineshapes for the electron modes are described by the sum of two Crystal Ball functions [31] with common mean peak position and different width and tail parameters. The lineshapes are determined separately in three bremsstrahlung categories, depending on whether none, one or both electrons are associated with bremsstrahlung photons. The width and tail parameters of these distributions, as well as the fractions of each bremsstrahlung category, are determined from simulation. In order to account for residual differences in the signal shape between data and simulation, an offset in the peak position and a scaling of the resolution are allowed to vary in the fits to the data. The muon decay mode is described with a Gaussian and the sum of two Crystal Ball functions. The shape parameters of these distributions are determined from simulation, with an offset in the peak position and scaling of the resolution allowed.

The combinatorial background is expected to follow an exponential shape as a function of the invariant mass in the case of the muon channel. However, due to the significantly worse resolution of the dilepton invariant mass in the electron channel, the  $\phi$  mass constraint

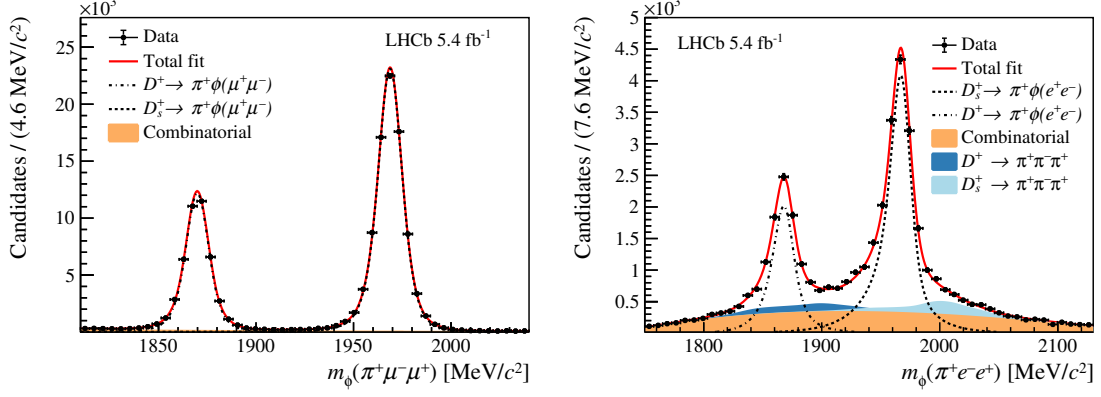


Figure 1: Distribution of the invariant mass  $m_\phi(\pi^+\ell^+\ell^-)$  overlaid with the result of the fit for candidates with (left) muon and (right) electron pairs in the final states. The dotted and dot-dashed lines describe the signal contributions, while the solid areas represent the background components.

induces a strong variation of the efficiency as a function of  $m_\phi(\pi^+\ell^+\ell^-)$  near the boundaries of the  $\pi^+\ell^+\ell^-$  invariant mass selection requirement (1770–2070 MeV/ $c^2$ ) in the trigger. Therefore, the combinatorial background for the electron mode is parameterised by a third-order polynomial. This parameterisation is verified on a sample of candidates with leptons of same charge (same-sign) and a sample where the BDT classifier requirement is inverted to favour the combinatorial background, as shown in Fig. 2 (left).

The dominant peaking background originates from  $D_{(s)}^+ \rightarrow \pi^+\pi^-\pi^+$  decays, where two pions are misidentified as either two muons or two electrons. Due to the narrow  $\phi$  mass window and the high rejection rate of the muon identification requirements, the contribution from this source in the muon mode is negligible. In the electron case, the

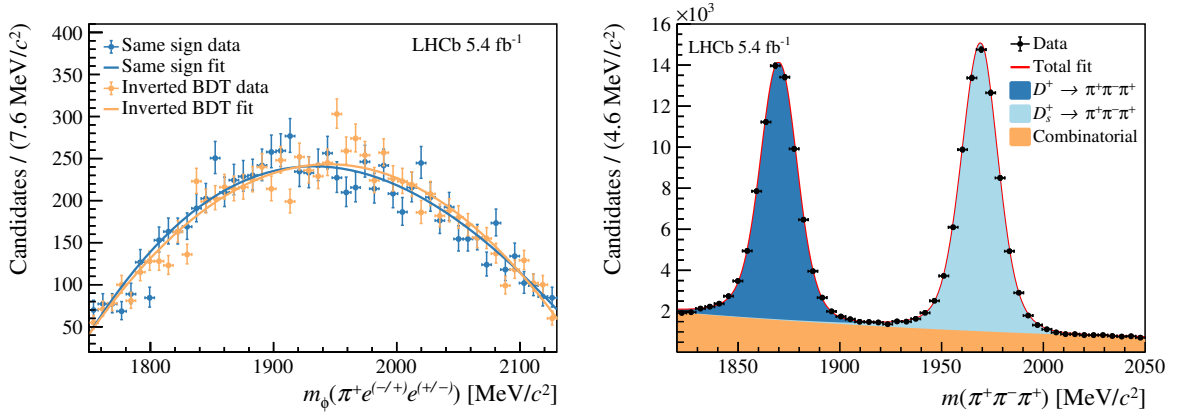


Figure 2: Left: distribution of the  $\pi^+\ell^+\ell^-$  invariant mass of candidates obtained from selecting final states with electrons of same charge (blue) or that fail the BDT requirement (orange). Fit results using a third-order polynomial are overlaid. The overall normalisation is chosen such that the two curves have the same area. Right: distribution of the invariant mass of  $\pi^+\ell^-\ell^+$  candidates, after interpreting the leptons as pions, for candidates failing the electron PID criteria. The reversed PID sample contains predominantly  $D_{(s)}^+ \rightarrow \pi^+\pi^-\pi^+$  events and a fraction of combinatorial events.

size and shape of this background are obtained by reversing the electron identification requirements in data. A fit to the invariant-mass distribution of candidates that fail the PID criteria is used to distinguish  $D^+$  and  $D_s^+$  contributions from combinatorial background in the reversed electron ID sample. The invariant mass is computed using the relevant mass hypothesis for each track. The result of this fit is shown in Fig. 2 (right). The *sPlot* [32] weights resulting from this fit and the misidentification (misID) probabilities from data are employed to translate the sample lineshape and yield to the signal region, obtaining a model for the doubly misidentified background component. In the signal-yield determination fit, the yield of this background component is constrained using a Gaussian penalty function to the value obtained using the data-driven misID probabilities. The validity of this procedure is verified with a dedicated study described in Sect. 6.

The yields of the normalisation modes are determined via a maximum-likelihood fit to the  $m_{J/\psi}(K^+\ell^+\ell^-)$  distribution, as shown in Fig. 3. By analogy to the signal decays, the mass is obtained with the dilepton invariant mass constrained to the known  $J/\psi$  mass. This procedure vastly improves the resolution for both the electron and muon channels. The lineshapes for the normalisation channels are described with the same parameterisation as for the signal channels. Unlike the  $\phi$  meson, the  $J/\psi$  meson has a negligible natural width compared to the resolution, therefore the combinatorial background shape is unaffected by the  $J/\psi$  mass constraint, and is described with an exponential function. Due to the worse resolution of the electron channel, the dominant background in the electron mode comes from partially reconstructed  $B^{(0,+)} \rightarrow K^+\pi^{(-,0)}J/\psi(\rightarrow e^+e^-)$  decays, where the pion is not included in the  $B^+$  candidate. The lineshape of this component is obtained from simulation, while its yield is free to float in the fit. A small contribution from misidentified  $B^+ \rightarrow (J/\psi \rightarrow \ell^+\ell^-)\pi^+$  background is included on the right-hand side of both muon and electron signal peaks. Their shape is obtained from simulation and their yield is constrained to the value obtained using the data-driven misID probabilities. The small disagreement near  $5400 \text{ MeV}/c^2$  in the muon mode has a negligible impact on the signal-yield determination.

The total yields are obtained summing over the fit results for different trigger categories

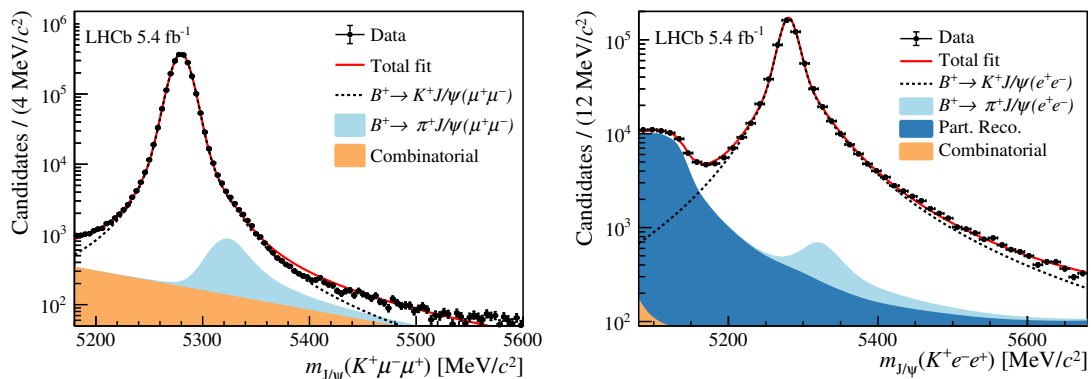


Figure 3: Invariant mass distributions of the selected candidates for the (left)  $B^+ \rightarrow K^+ J/\psi(\rightarrow e^+e^-)$  and (right)  $B^+ \rightarrow K^+ J/\psi(\rightarrow \mu^+\mu^-)$  modes, overlaid with the result of the fit. The dotted lines describe the signal contribution and the solid areas represent each of the background components described in the text.



and run periods, and are summarised in Table 2. In the muon channel, the correlation between the  $D^+ \rightarrow \pi^+\phi$  and  $D_s^+ \rightarrow \pi^+\phi$  yields is negligible, while in the electron channel the two yields are correlated by 30–45%, depending on the trigger category, due to the worse mass resolution for electrons.

## 5 Efficiency calculation

The yields in Table 2 are used to compute  $R_{\phi\pi}^{(d,s)}$  according to the definition

$$R_{\phi\pi}^{(d,s)} = \frac{N^{(d,s)}(\pi^+\phi(\rightarrow \mu^+\mu^-)) \varepsilon^{(d,s)}(\pi^+\phi(\rightarrow e^+e^-))}{N^{(d,s)}(\pi^+\phi(\rightarrow e^+e^-)) \varepsilon^{(d,s)}(\pi^+\phi(\rightarrow \mu^+\mu^-))} / r_{J/\psi}, \quad (2)$$

where  $N^{(d,s)}(X)$  and  $\varepsilon^{(d,s)}(X)$  are the yields and efficiencies to detect the decay  $X$  initiated by a  $D_{(s)}^+$  meson. The relative electron to muon efficiencies for signal and normalisation channels are determined from simulation. The efficiencies for each run period are obtained from a direct sum over the efficiency in each trigger category. The total efficiency for each channel is obtained by performing a luminosity-weighted average in the different run periods and are combined with the yields in Table 2 to derive the final result.

The simulation has several data-driven corrections applied, largely following the procedure used for the  $R_K$  measurement described in Ref. [6], where each correction is applied with respect to the preceding one.

Firstly, the tracking efficiency for electrons is determined using a tag-and-probe method applied to a  $B^+ \rightarrow K^+ J/\psi(\rightarrow e^+e^-)$  sample [33]. The difference in tracking efficiency between data and simulated samples, as a function of the pseudorapidity, the azimuthal angle  $\phi$  and the  $p_T$  of the probe particle, is corrected for. The effect of these corrections is less than 1%, reflecting the good agreement between simulation and data.

The PID efficiency is obtained from simulation using a set of control channels in data that can be efficiently selected without the application of PID criteria. These samples include the decays  $D^{*+} \rightarrow D^0\pi^+$  for hadron identification and  $h \rightarrow \ell$  misID and  $B^+ \rightarrow K^+ J/\psi(\rightarrow \mu^+\mu^-)$  for muon identification. The PID distribution in data is obtained using the *sPlot* procedure [34] as a function of the muon transverse momentum and pseudorapidity. The fraction of these distributions above the PID selection criteria are then used as PID efficiencies determined from data. For the electron PID response, the efficiencies are determined by refitting the signal  $B^+ \rightarrow K^+ J/\psi(\rightarrow e^+e^-)$  yield before

Table 2: Yields of the signal and normalisation decay modes obtained from the fits to the data. The quoted uncertainty accounts for both statistical and systematic effects.

Decay mode	Yield
$D^+ \rightarrow \pi^+\phi(\rightarrow e^+e^-)$	$7\,460 \pm 140$
$D^+ \rightarrow \pi^+\phi(\rightarrow \mu^+\mu^-)$	$43\,512 \pm 220$
$D_s^+ \rightarrow \pi^+\phi(\rightarrow e^+e^-)$	$16\,740 \pm 210$
$D_s^+ \rightarrow \pi^+\phi(\rightarrow \mu^+\mu^-)$	$87\,022 \pm 300$
$B^+ \rightarrow K^+ J/\psi(\rightarrow e^+e^-)$	$638\,600 \pm 900$
$B^+ \rightarrow K^+ J/\psi(\rightarrow \mu^+\mu^-)$	$2\,187\,000 \pm 1\,500$

and after the PID selection in bins of kinematic variables and bremsstrahlung recovery category, therefore taking into account differences in the background shape as a function of the PID response. The correction due to the assumption of factorisation of per-electron PID efficiencies is determined using simulation and is found to have a  $<0.1\%$  effect on the overall efficiency.

An initial set of corrections that are designed to account for the mis-modelling of the production kinematics and vertex quality in the simulation are applied. These corrections are obtained using the muon channels and applied to both muon and electron channels after the PID and tracking corrections have been applied. The corrections comprise a two-dimensional correction as a function of the  $B^+$  and  $D_{(s)}^+$  transverse momentum and pseudorapidity, followed by a one-dimensional correction to the quality of the fits to the  $B^+$  and  $D_{(s)}^+$  decay vertices. These corrections are applied iteratively to account for the correlation between the vertex quality and the production kinematics. Only two iterations are needed to obtain a satisfactory agreement in all three variables. The corrections to the efficiencies discussed below are obtained after applying these initial corrections to the simulation.

The largest efficiency difference between muons and electrons in the experiment originates from the trigger, where the  $p_T$  requirement for electrons is significantly more restrictive than for muons. Even when combining the three electron trigger categories, the total trigger efficiency of the electron channel is around 20% of the muon channel. The normalisation channel is used to compare the trigger response between data and simulation, via a tag-and-probe method. For example, the kaon from the  $B^+ \rightarrow K^+ J/\psi (\rightarrow e^+ e^-)$  decay, referred to as the tag, is required to pass a set of trigger requirements. The efficiency of the electron trigger is then determined by the fraction of candidates where either of the two electrons is also selected by the trigger. This efficiency is compared between data and simulation as a function of the maximum  $p_T$  of the two electrons, which is expected to be the kinematic variable on which the electron trigger efficiency most strongly depends. The efficiency for the hadron and muon triggers are determined in a similar way, as a function of the  $p_T$  of the kaon or muon. The discrepancy between measured and simulated efficiencies to trigger independently of the signal, is corrected differently, depending on the particle species that fired the trigger. For events triggered by any muon or hadron that are not part of the signal candidate, the trigger efficiency is parametrised in terms of the transverse momentum of the  $B$  meson, while for events triggered by an electron or a photon which are not part of the signal, the maximum  $p_T$  of the dilepton pair is used.

A final set of corrections is obtained to correct for any residual mismodelling of the efficiencies as a function of the  $B^+(D_{(s)}^+)$  production kinematic and geometrical quantities. Similar to the initial corrections, an iterative reweighting procedure is applied as a function of the  $B^+(D_{(s)}^+)$   $p_T$  and pseudorapidity, the  $B^+(D_{(s)}^+)$  vertex-fit quality and the  $\chi_{\text{IP}}^2$  with respect to the associated PV, where  $\chi_{\text{IP}}^2$  is defined as the difference in the vertex-fit  $\chi^2$  of the PV reconstructed with and without the considered particle. These corrections are obtained using the muon channels, and are assumed to be independent of the lepton species and trigger category. This set of corrections is obtained after having accounted for the mismodelling of the PID and trigger efficiencies in the electron modes as well, enabling evaluation of the systematic uncertainty due to these assumptions.

Finally, the dilepton invariant mass distribution is compared between data and simulation for  $B^+ \rightarrow K^+ J/\psi (\rightarrow e^+ e^-)$  candidates. The dilepton invariant mass distribution of simulated events is fitted with a double-sided Crystal Ball [31] function. This shape is

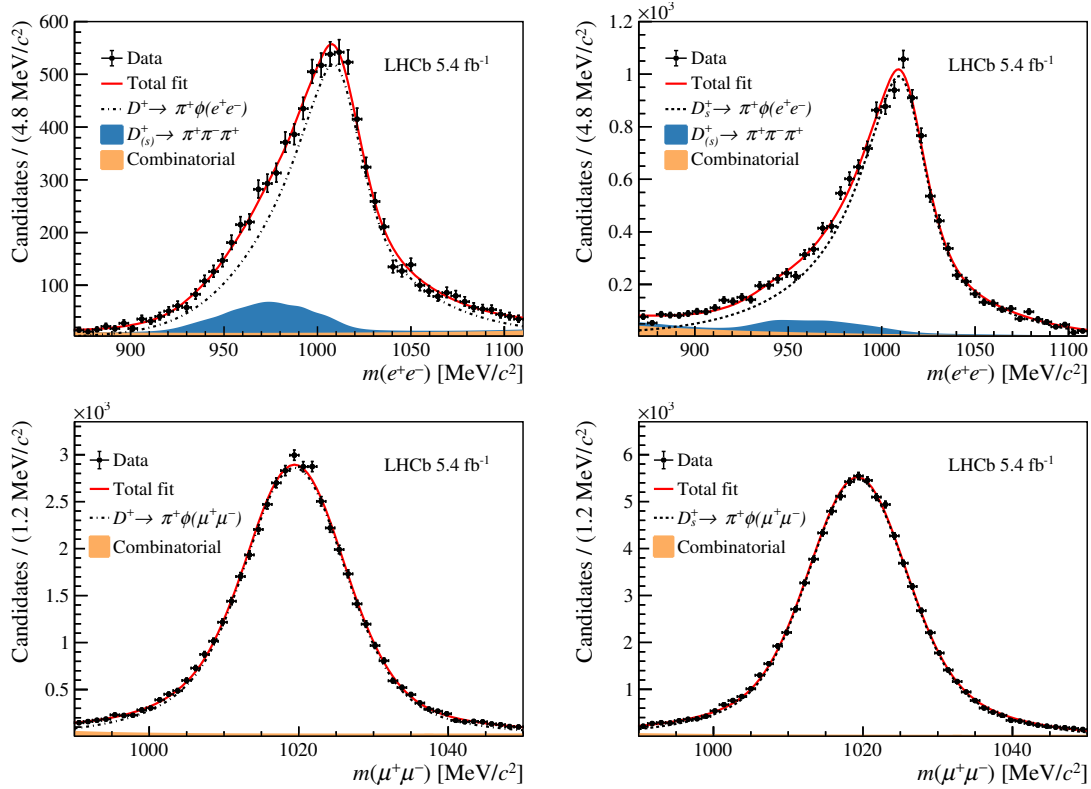


Figure 4: Distributions of (top)  $m(e^+e^-)$  and (bottom)  $m(\mu^+\mu^-)$  for candidates selected in the signal region of the (left)  $D^+$  (right) and  $D_s^+$   $\phi$ -constrained invariant mass. The dotted lines describe the signal contribution and the solid areas represent each of the background components described in the text.

then used to fit the data distribution with the mean and scale parameters, representing the mismatch between simulated and measured  $q^2$  resolution, allowed to vary in the fit. These resolution parameters are determined as a function of the number of recovered bremsstrahlung photons and the trigger category. Overall, the resolution in the data is found to be 10–20% worse than in simulation, with a shift in the peak position of around 2–10  $\text{MeV}/c^2$ , depending on the trigger category. This resolution correction is applied to the  $q^2$  and  $B^+(D_{(s)}^+)$  invariant mass distributions of both normalisation and signal channels. This correction affects the shape of invariant mass distributions and therefore the efficiency of the invariant-mass requirements. The correction is derived assuming that the smearing parameters are independent of the electron pair momentum and the detector occupancy. Due to the stringent requirement on the  $\pi^+\ell^+\ell^-$  invariant mass in the trigger, assumptions associated with the resolution in the electron channel constitute one of the largest systematic uncertainties in the measurement.

A fit to the dilepton mass distribution without any kinematic constraints is shown in Fig. 4 for signal candidates selected in a narrow  $m_\phi(\pi^+\ell^+\ell^-)$  window around the known  $D^+$  and  $D_s^+$  masses. The signal shape is divided into categories based on the number of bremsstrahlung photons recovered, each modelled by a double-sided Crystal Ball function. The parameters of these distributions are obtained from a fit to the smeared distributions of simulated candidates. The agreement between the shapes obtained from simulation and the data provides a validation of the resolution description at low  $q^2$ .

Table 3: Relative systematic uncertainties in percent affecting the measurements  $R_{\phi\pi}^d$  and  $R_{\phi\pi}^s$ .

Source	$R_{\phi\pi}^d$ [%]	$R_{\phi\pi}^s$ [%]
Resolution on $q^2$	4.0	3.9
Event multiplicity	2.7	2.7
Simulation reweighting	1.5	1.2
Combinatorial background shape parametrisation	1.5	1.0
PID	0.8	0.8
Finite size of control samples	0.8	0.6
Trigger	0.3	0.3
Tracking	0.1	0.1
Background from doubly misidentified electrons	1.1	0.1
Total	5.5	5.1

## 6 Systematic uncertainties

A summary of the systematic uncertainties is given in Table 3. Systematic uncertainties associated with the assumptions in the analysis are determined using variations of the result under alternative methods. The standard deviation of these variations is assigned as a systematic uncertainty. The systematic sources are assumed to be uncorrelated.

The assumptions used to correct the imperfect simulation of the dielectron  $q^2$  resolution lead to the largest systematic uncertainty in the measurement. The nominal resolution smearing parameters are assumed to be independent of the electron momenta. To account for the systematic uncertainty arising from this assumption, the simulated  $q^2$  and  $B^+(D_{(s)}^+)$  distributions are corrected by measuring the resolution in data for the normalisation channel as a function of the electron pair momentum. In addition, an alternative resolution smearing procedure is used, which depends on the number of hits reconstructed in the SPD. The sample is divided into three equally populated regions according to the number of SPD hits, and separate smearing parameters are obtained for each region. Additional uncertainties arising from the limited precision of the resolution parameters are found to have a negligible effect.

The particle multiplicity is mismodelled in the simulation. For example, there are around 10% fewer tracks per event and around 30% fewer hits in the SPD reconstructed in simulation compared to the data. A systematic correction associated to this mismodelling is determined by adding to the initial set of corrections a separate reweighting of three different multiplicity proxies: the number of fully reconstructed tracks, the number of primary vertices reconstructed in the VELO and the number of hits reconstructed in the SPD. Although only weakly correlated between different lepton flavours, this leads to a large systematic uncertainty due to the mismodelling of the SPD multiplicity and the different production mechanisms for the signal and normalisation channels.

The final set of corrections is obtained from the muon channels and is applied coherently to both electron and muon channels. A systematic uncertainty based on the assumption that the corrections are independent of lepton flavour is determined by obtaining the corrections from the  $B^+ \rightarrow K^+ J/\psi (\rightarrow e^+ e^-)$  channel instead. An additional set of mixed corrections is also derived, whereby the production corrections originate from the muon

control channels and the vertex quality and IP  $\chi^2$  originate from the electron control channels, and are then applied to the signal channel. The impact of the trigger on the weights applied to correct the simulation is determined by varying the trigger requirement for the samples used in those corrections.

Three alternative methods for extracting the signal yields are adopted to determine the systematic uncertainty arising from the combinatorial background parameterisation for the electron mode. Firstly, the coefficients describing the combinatorial shape in the fit are constrained to the values obtained from two independent proxies: a sample where the two reconstructed leptons have the same charge and a sample where the BDT requirement is reversed. Secondly, the assumption arising from the truncation of the polynomial is relaxed by increasing it to fourth order.

Three systematic sources are considered for the determination of the PID efficiencies: the binning scheme of the PID response as a function of the kinematic variables; the dependence of the PID response on the trigger; and the assumption that the PID response factorises between the two electrons. As the PID selection is highly efficient, these assumptions result in a small systematic uncertainty. A comparably small uncertainty is associated with the tracking efficiency corrections.

The limited size of the control samples used to derive corrections to the simulated efficiencies gives rise to an associated systematic uncertainty. The impact of this is determined by bootstrapping [35] the relevant samples and re-computing the associated efficiencies. The 68% envelope of these repeated efficiency determinations is assigned as the systematic uncertainty.

The systematic uncertainty associated with the trigger corrections originates from the dependence on the requirement on the tag lepton used in the tag-and-probe method. This is determined by varying this tag requirement, where the largest effects are seen in the hadronic trigger category. The assumption that the trigger efficiencies factorise between the two electrons is also determined by parameterising the trigger response as a function of the distance between the electron clusters in the ECAL.

In the nominal signal-yield determination, the estimate of the doubly misidentified background relies on the translation of this background source from the reversed PID region to the signal PID region using the known PID efficiencies. An alternative procedure that does not rely on this method is used to extract the signal yields, and the difference between these results is taken as a systematic uncertainty. In the alternative signal extraction procedure, the expected  $D_{(s)}^+ \rightarrow \pi^+\pi^-\pi^+$  contamination is obtained from a fit to the  $\pi\pi\pi$  invariant-mass distribution for signal candidates selected in the signal PID region, such that no translation across PID regions is needed. The result of the fit is shown in Fig. 5. In this alternative approach, the contamination of doubly misidentified background events is constrained to the one extracted from the nominal PID region fit. This leads to a comparatively larger systematic uncertainty for the  $D^+ \rightarrow \pi^+\phi$  mode compared to the  $D_s^+ \rightarrow \pi^+\phi$  decay as the misID background peaks in the vicinity of the  $D^+$  mass. The small size of this systematic uncertainty confirms the accuracy of data-driven estimates of the misidentified  $h \rightarrow e$  background sources in LFU analyses at low  $q^2$ .

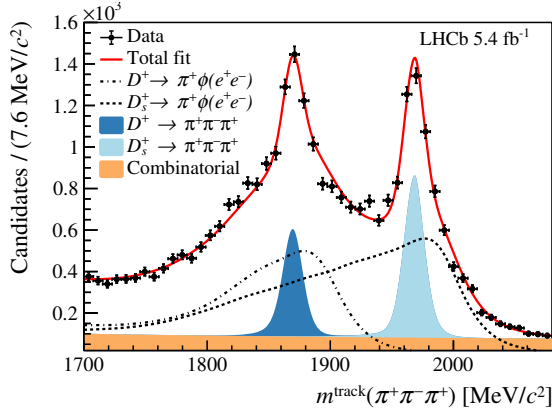


Figure 5: Distribution of the invariant mass computed under the pion mass hypothesis for the dielectron pair using track information only, for candidates passing the electron PID criteria. The fit projection is superimposed, with dashed and dotted-dashed lines describing the signal contributions, while solid light and dark blue areas represent misidentified  $D_{(s)}^+ \rightarrow \pi^+ \pi^- \pi^+$  components. In this variable the latter are clearly visible in data passing the electron PID criteria.

## 7 Results and conclusion

The final results are

$$R_{\phi\pi}^d = 1.026 \pm 0.020 \text{ (stat)} \pm 0.056 \text{ (syst)},$$

$$R_{\phi\pi}^s = 1.017 \pm 0.013 \text{ (stat)} \pm 0.051 \text{ (syst)}.$$

A combination of the ratios from the two charm hadron decays is obtained by performing a weighted average of the two results, taking into account the correlations

$$R_{\phi\pi} = 1.022 \pm 0.012 \text{ (stat)} \pm 0.048 \text{ (syst)}.$$

This result is combined with the existing  $\phi \rightarrow e^+ e^-$  branching fraction measurement of  $(2.979 \pm 0.033) \times 10^{-4}$  [9] to obtain a measurement of

$$\mathcal{B}(\phi \rightarrow \mu^+ \mu^-) = (3.045 \pm 0.049 \text{ (stat)} \pm 0.148 \text{ (syst)}) \times 10^{-4},$$

This is the most precise measurement of this branching fraction to date.

These results are compatible with previous measurements [9] and with lepton flavour universality at less than one standard deviation. Systematic uncertainties related to the efficiency determination are larger than those in the  $R_K$  and  $R_{K^*}$  analyses [1, 2] due to the different production mechanism between the signal and normalisation channels and restrictive invariant mass requirements in the trigger. This restriction only affects the charm decays analysed in this measurement and can be improved in the future. In addition, the variation of the measured value as a function of several kinematic variables is shown in Fig. 6. No significant dependence on these variables is observed. Assuming the fluctuations seen in these variables are attributed to a systematic effect, the maximum deviation in the efficiency is found to be 2.5%, which shows that the efficiency of electrons can be controlled at least at this level for low-mass di-electron signatures.

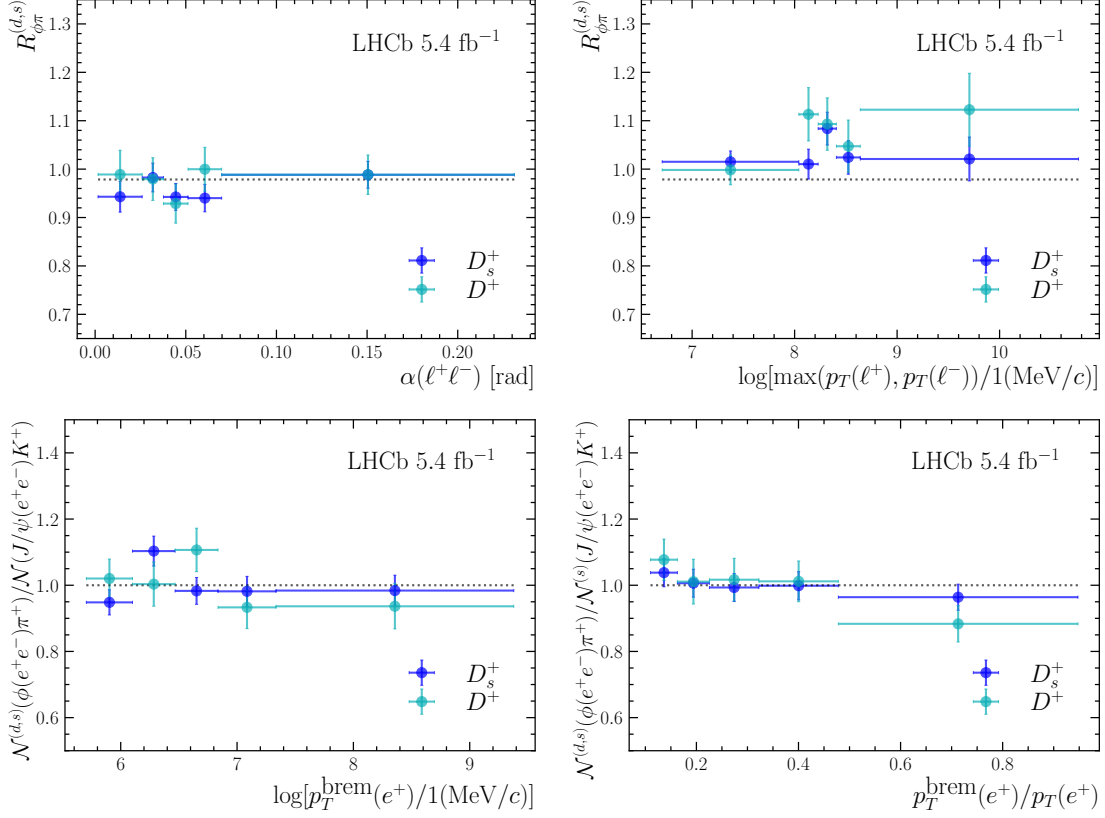


Figure 6: Measured  $R_{\phi\pi}^{(d,s)}$  as a function of the (top left) angle between the leptons  $\alpha(\ell^+, \ell^-)$ , and (top right) the maximum  $p_T$  of the leptons. The structure observed at intermediate maximum  $p_T$  is related to the trigger threshold. The errors shown are statistical only. Also shown is the ratio of efficiency-corrected  $D_{(s)}^+ \rightarrow \pi^+\phi$  and  $B^+ \rightarrow K^+ J/\psi(\rightarrow e^+e^-)$  yields as a function of the (bottom left) transverse momentum recovered with the bremsstrahlung recovery algorithm and (bottom right) its fraction with respect to the total transverse momentum of the electron. The flatness of these distributions indicates that the bremsstrahlung recovery algorithm is well reproduced in simulation at low  $q^2$ . The normalisation of these distributions is arbitrary and the uncertainties displayed are statistical only.

Similar to the  $R_{K^{(*)}}$  measurements [1, 2], the single ratio of the normalisation channel  $r_{J/\psi}$  is determined to cross-check the efficiency correction procedure. This is found to be compatible with the SM at the level of 0.6 sigma and with previous analyses. Such agreement is expected, as a very similar correction procedure is applied in this case.

In summary, the branching fraction ratio  $\mathcal{B}(\phi \rightarrow \mu^+\mu^-)/\mathcal{B}(\phi \rightarrow e^+e^-)$  is determined with  $D^+ \rightarrow \pi^+\phi$  and  $D_s^+ \rightarrow \pi^+\phi$  decays, using a dataset corresponding to an integrated luminosity of  $5.4 \text{ fb}^{-1}$  of  $pp$  collision data collected with the LHCb experiment. The results are consistent with the Standard Model and with previous measurements. This is the first lepton flavour universality test in  $\phi$  meson decays at the LHCb experiment. It probes a unique kinematic region and is crucial for understanding the experimental features of low-mass dileptons in the LHCb environment.

# Acknowledgements

We express our gratitude to our colleagues in the CERN accelerator departments for the excellent performance of the LHC. We thank the technical and administrative staff at the LHCb institutes. We acknowledge support from CERN and from the national agencies: CAPES, CNPq, FAPERJ and FINEP (Brazil); MOST and NSFC (China); CNRS/IN2P3 (France); BMBF, DFG and MPG (Germany); INFN (Italy); NWO (Netherlands); MNiSW and NCN (Poland); MCID/IFA (Romania); MICINN (Spain); SNSF and SER (Switzerland); NASU (Ukraine); STFC (United Kingdom); DOE NP and NSF (USA). We acknowledge the computing resources that are provided by CERN, IN2P3 (France), KIT and DESY (Germany), INFN (Italy), SURF (Netherlands), PIC (Spain), GridPP (United Kingdom), CSCS (Switzerland), IFIN-HH (Romania), CBPF (Brazil), and Polish WLCG (Poland). We are indebted to the communities behind the multiple open-source software packages on which we depend. Individual groups or members have received support from ARC and ARDC (Australia); Key Research Program of Frontier Sciences of CAS, CAS PIFI, CAS CCEPP, Fundamental Research Funds for the Central Universities, and Sci. & Tech. Program of Guangzhou (China); Minciencias (Colombia); EPLANET, Marie Skłodowska-Curie Actions, ERC and NextGenerationEU (European Union); A\*MIDEX, ANR, IPhU and Labex P2IO, and Région Auvergne-Rhône-Alpes (France); AvH Foundation (Germany); ICSC (Italy); GVA, XuntaGal, GENCAT, Inditex, InTalent and Prog. Atracción Talento, CM (Spain); SRC (Sweden); the Leverhulme Trust, the Royal Society and UKRI (United Kingdom).

# References

- [1] LHCb collaboration, R. Aaij *et al.*, *Test of lepton universality in  $b \rightarrow s\ell^+\ell^-$  decays*, Phys. Rev. Lett. **131** (2023) 051803, [arXiv:2212.09152](#).
- [2] LHCb collaboration, R. Aaij *et al.*, *Measurement of lepton universality parameters in  $B^+ \rightarrow K^+\ell^+\ell^-$  and  $B^0 \rightarrow K^{*0}\ell^+\ell^-$  decays*, Phys. Rev. **D108** (2023) 032002, [arXiv:2212.09153](#).
- [3] LHCb collaboration, R. Aaij *et al.*, *Test of lepton universality using  $B^+ \rightarrow K^+\ell^+\ell^-$  decays*, Phys. Rev. Lett. **113** (2014) 151601, [arXiv:1406.6482](#).
- [4] LHCb collaboration, R. Aaij *et al.*, *Test of lepton universality with  $B^0 \rightarrow K^{*0}\ell^+\ell^-$  decays*, JHEP **08** (2017) 055, [arXiv:1705.05802](#).
- [5] LHCb collaboration, R. Aaij *et al.*, *Search for lepton-universality violation in  $B^+ \rightarrow K^+\ell^+\ell^-$  decays*, Phys. Rev. Lett. **122** (2019) 191801, [arXiv:1903.09252](#).
- [6] LHCb collaboration, R. Aaij *et al.*, *Test of lepton universality in beauty-quark decays*, Nature Physics **18** (2022) 277, [arXiv:2103.11769](#).
- [7] LHCb collaboration, R. Aaij *et al.*, *Tests of lepton universality using  $B^0 \rightarrow K_S^0\ell^+\ell^-$  and  $B^+ \rightarrow K^{*+}\ell^+\ell^-$  decays*, Phys. Rev. Lett. **128** (2022) 191802, [arXiv:2110.09501](#).
- [8] W. Altmannshofer *et al.*, *Light resonances and the low- $q^2$  bin of  $R_{K^*}$* , JHEP **03** (2018) 188, [arXiv:1711.07494](#).



- [9] Particle Data Group, R. L. Workman *et al.*, *Review of particle physics*, Prog. Theor. Exp. Phys. **2022** (2022) 083C01.
- [10] R. R. Akhmetshin *et al.*, *Measurement of phi meson parameters with CMD-2 detector at VEPP-2M collider*, Phys. Lett. **B364** (1995) 199.
- [11] R. R. Akhmetshin *et al.*, *Measurement of  $\phi(1020)$  meson leptonic width with CMD-2 detector at VEPP-2M Collider*, Phys. Lett. **B695** (2011) 412, arXiv:1010.4878.
- [12] KLOE collaboration, F. Ambrosino *et al.*, *Measurement of the leptonic decay widths of the phi-meson with the KLOE detector*, Phys. Lett. **B608** (2005) 199, arXiv:hep-ex/0411082.
- [13] LHCb collaboration, A. A. Alves Jr. *et al.*, *The LHCb detector at the LHC*, JINST **3** (2008) S08005.
- [14] LHCb collaboration, R. Aaij *et al.*, *LHCb detector performance*, Int. J. Mod. Phys. **A30** (2015) 1530022, arXiv:1412.6352.
- [15] R. Aaij *et al.*, *Performance of the LHCb Vertex Locator*, JINST **9** (2014) P09007, arXiv:1405.7808.
- [16] P. d'Argent *et al.*, *Improved performance of the LHCb Outer Tracker in LHC Run 2*, JINST **12** (2017) P11016, arXiv:1708.00819.
- [17] M. Adinolfi *et al.*, *Performance of the LHCb RICH detector at the LHC*, Eur. Phys. J. **C73** (2013) 2431, arXiv:1211.6759.
- [18] A. A. Alves Jr. *et al.*, *Performance of the LHCb muon system*, JINST **8** (2013) P02022, arXiv:1211.1346.
- [19] T. Sjöstrand, S. Mrenna, and P. Skands, *A brief introduction to PYTHIA 8.1*, Comput. Phys. Commun. **178** (2008) 852, arXiv:0710.3820; T. Sjöstrand, S. Mrenna, and P. Skands, *PYTHIA 6.4 physics and manual*, JHEP **05** (2006) 026, arXiv:hep-ph/0603175.
- [20] I. Belyaev *et al.*, *Handling of the generation of primary events in Gauss, the LHCb simulation framework*, J. Phys. Conf. Ser. **331** (2011) 032047.
- [21] D. J. Lange, *The EvtGen particle decay simulation package*, Nucl. Instrum. Meth. **A462** (2001) 152.
- [22] N. Davidson, T. Przedzinski, and Z. Was, *PHOTOS interface in C++: Technical and physics documentation*, Comp. Phys. Comm. **199** (2016) 86, arXiv:1011.0937.
- [23] Geant4 collaboration, J. Allison *et al.*, *Geant4 developments and applications*, IEEE Trans. Nucl. Sci. **53** (2006) 270; Geant4 collaboration, S. Agostinelli *et al.*, *Geant4: A simulation toolkit*, Nucl. Instrum. Meth. **A506** (2003) 250.
- [24] M. Clemencic *et al.*, *The LHCb simulation application, Gauss: Design, evolution and experience*, J. Phys. Conf. Ser. **331** (2011) 032023.

- [25] R. Aaij *et al.*, *The LHCb trigger and its performance in 2011*, JINST **8** (2013) P04022, arXiv:1211.3055.
- [26] G. Dujany and B. Storaci, *Real-time alignment and calibration of the LHCb Detector in Run II*, J. Phys. Conf. Ser. **664** (2015) 082010.
- [27] R. Aaij *et al.*, *Tesla: an application for real-time data analysis in High Energy Physics*, Comput. Phys. Commun. **208** (2016) 35, arXiv:1604.05596.
- [28] L. Breiman, J. H. Friedman, R. A. Olshen, and C. J. Stone, *Classification and regression trees*, Wadsworth international group, Belmont, California, USA, 1984.
- [29] Y. Freund and R. E. Schapire, *A decision-theoretic generalization of on-line learning and an application to boosting*, J. Comput. Syst. Sci. **55** (1997) 119.
- [30] G. Punzi, *Sensitivity of searches for new signals and its optimization*, eConf **C030908** (2003) MODT002, arXiv:physics/0308063.
- [31] T. Skwarnicki, *A study of the radiative cascade transitions between the Upsilon-prime and Upsilon resonances*, PhD thesis, Institute of Nuclear Physics, Krakow, 1986, DESY-F31-86-02.
- [32] M. Pivk and F. R. Le Diberder, *sPlot: A statistical tool to unfold data distributions*, Nucl. Instrum. Meth. **A555** (2005) 356, arXiv:physics/0402083.
- [33] LHCb collaboration, R. Aaij *et al.*, *Measurement of the electron reconstruction efficiency at LHCb*, JINST **14** (2019) P11023, arXiv:1909.02957.
- [34] R. Aaij *et al.*, *Selection and processing of calibration samples to measure the particle identification performance of the LHCb experiment in Run 2*, Eur. Phys. J. Tech. Instr. **6** (2019) 1, arXiv:1803.00824.
- [35] B. Efron, *Bootstrap Methods: Another Look at the Jackknife*, The Annals of Statistics **7** (1979) 1 .







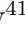
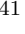






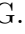



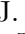
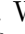




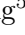


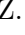



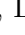
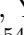


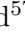
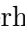

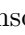




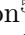
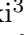





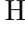

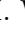
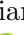


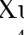
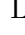

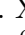


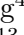

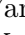














## LHCb collaboration

R. Aaij<sup>35</sup> , A.S.W. Abdelmotteleb<sup>54</sup> , C. Abellan Beteta<sup>48</sup> , F. Abudinén<sup>54</sup> ,  
T. Ackernley<sup>58</sup> , B. Adeva<sup>44</sup> , M. Adinolfi<sup>52</sup> , P. Adlarson<sup>78</sup> , C. Agapopoulou<sup>46</sup> ,  
C.A. Aidala<sup>79</sup> , Z. Ajaltouni<sup>11</sup> , S. Akar<sup>63</sup> , K. Akiba<sup>35</sup> , P. Albicocco<sup>25</sup> , J. Albrecht<sup>17</sup> ,  
F. Alessio<sup>46</sup> , M. Alexander<sup>57</sup> , A. Alfonso Albero<sup>43</sup> , Z. Aliouche<sup>60</sup> ,  
P. Alvarez Cartelle<sup>53</sup> , R. Amalric<sup>15</sup> , S. Amato<sup>3</sup> , J.L. Amey<sup>52</sup> , Y. Amhis<sup>13,46</sup> ,  
L. An<sup>6</sup> , L. Anderlini<sup>24</sup> , M. Andersson<sup>48</sup> , A. Andreianov<sup>41</sup> , P. Andreola<sup>48</sup> ,  
M. Andreotti<sup>23</sup> , D. Andreou<sup>66</sup> , A. Anelli<sup>28,o</sup> , D. Ao<sup>7</sup> , F. Archilli<sup>34,u</sup> ,  
M. Argenton<sup>23</sup> , S. Arguedas Cuendis<sup>9</sup> , A. Artamonov<sup>41</sup> , M. Artuso<sup>66</sup> ,  
E. Aslanides<sup>12</sup> , M. Atzeni<sup>62</sup> , B. Audurier<sup>14</sup> , D. Bacher<sup>61</sup> , I. Bachiller Perea<sup>10</sup> ,  
S. Bachmann<sup>19</sup> , M. Bachmayer<sup>47</sup> , J.J. Back<sup>54</sup> , P. Baladron Rodriguez<sup>44</sup> ,  
V. Balagura<sup>14</sup> , W. Baldini<sup>23</sup> , J. Baptista de Souza Leite<sup>2</sup> , M. Barbetti<sup>24,l</sup> , I.  
R. Barbosa<sup>67</sup> , R.J. Barlow<sup>60</sup> , S. Barsuk<sup>13</sup> , W. Barter<sup>56</sup> , M. Bartolini<sup>53</sup> ,  
J. Bartz<sup>66</sup> , F. Baryshnikov<sup>41</sup> , J.M. Basels<sup>16</sup> , G. Bassi<sup>32,r</sup> , B. Batsukh<sup>5</sup> ,  
A. Battig<sup>17</sup> , A. Bay<sup>47</sup> , A. Beck<sup>54</sup> , M. Becker<sup>17</sup> , F. Bedeschi<sup>32</sup> , I.B. Bediaga<sup>2</sup> ,  
A. Beiter<sup>66</sup> , S. Belin<sup>44</sup> , V. Bellee<sup>48</sup> , K. Belous<sup>41</sup> , I. Belov<sup>26</sup> , I. Belyaev<sup>41</sup> ,  
G. Benane<sup>12</sup> , G. Bencivenni<sup>25</sup> , E. Ben-Haim<sup>15</sup> , A. Berezhnoy<sup>41</sup> , R. Bernet<sup>48</sup> ,  
S. Bernet Andres<sup>42</sup> , H.C. Bernstein<sup>66</sup> , C. Bertella<sup>60</sup> , A. Bertolin<sup>30</sup> , C. Betancourt<sup>48</sup> ,  
F. Betti<sup>56</sup> , J. Bex<sup>53</sup> , I.a. Bezshyiko<sup>48</sup> , J. Bhom<sup>38</sup> , M.S. Bieker<sup>17</sup> , N.V. Biesuz<sup>23</sup> ,  
P. Billoir<sup>15</sup> , A. Biolchini<sup>35</sup> , M. Birch<sup>59</sup> , F.C.R. Bishop<sup>10</sup> , A. Bitadze<sup>60</sup> ,  
A. Bizzeti , M.P. Blago<sup>53</sup> , T. Blake<sup>54</sup> , F. Blanc<sup>47</sup> , J.E. Blank<sup>17</sup> , S. Blusk<sup>66</sup> ,  
D. Bobulska<sup>57</sup> , V. Bocharnikov<sup>41</sup> , J.A. Boelhauve<sup>17</sup> , O. Boente Garcia<sup>14</sup> ,  
T. Boettcher<sup>63</sup> , A. Bohare<sup>56</sup> , A. Boldyrev<sup>41</sup> , C.S. Bolognani<sup>76</sup> , R. Bolzonella<sup>23,k</sup> ,  
N. Bondar<sup>41</sup> , F. Borgato<sup>30,46</sup> , S. Borghi<sup>60</sup> , M. Borsato<sup>28,o</sup> , J.T. Borsuk<sup>38</sup> ,  
S.A. Bouchiba<sup>47</sup> , T.J.V. Bowcock<sup>58</sup> , A. Boyer<sup>46</sup> , C. Bozzi<sup>23</sup> , M.J. Bradley<sup>59</sup>,  
S. Braun<sup>64</sup> , A. Brea Rodriguez<sup>44</sup> , N. Breer<sup>17</sup> , J. Brodzicka<sup>38</sup> , A. Brossa Gonzalo<sup>44</sup> ,  
J. Brown<sup>58</sup> , D. Brundu<sup>29</sup> , A. Buonauro<sup>48</sup> , L. Buonincontri<sup>30</sup> , A.T. Burke<sup>60</sup> ,  
C. Burr<sup>46</sup> , A. Bursche<sup>69</sup> , A. Butkevich<sup>41</sup> , J.S. Butter<sup>53</sup> , J. Buytaert<sup>46</sup> ,  
W. Byczynski<sup>46</sup> , S. Cadeddu<sup>29</sup> , H. Cai<sup>71</sup> , R. Calabrese<sup>23,k</sup> , L. Calefice<sup>17</sup> , S. Cali<sup>25</sup> ,  
M. Calvi<sup>28,o</sup> , M. Calvo Gomez<sup>42</sup> , J. Cambon Bouzas<sup>44</sup> , P. Campana<sup>25</sup> ,  
D.H. Campora Perez<sup>76</sup> , A.F. Campoverde Quezada<sup>7</sup> , S. Capelli<sup>28,o</sup> , L. Capriotti<sup>23</sup> ,  
R. Caravaca-Mora<sup>9</sup> , A. Carbone<sup>22,i</sup> , L. Carcedo Salgado<sup>44</sup> , R. Cardinale<sup>26,m</sup> ,  
A. Cardini<sup>29</sup> , P. Carniti<sup>28,o</sup> , L. Carus<sup>19</sup> , A. Casais Vidal<sup>62</sup> , R. Caspary<sup>19</sup> ,  
G. Casse<sup>58</sup> , J. Castro Godinez<sup>9</sup> , M. Cattaneo<sup>46</sup> , G. Cavallero<sup>23</sup> , V. Cavallini<sup>23,k</sup> ,  
S. Celani<sup>47</sup> , J. Cerasoli<sup>12</sup> , D. Cervenkov<sup>61</sup> , S. Cesare<sup>27,n</sup> , A.J. Chadwick<sup>58</sup> ,  
I. Chahrouh<sup>79</sup> , M. Charles<sup>15</sup> , Ph. Charpentier<sup>46</sup> , C.A. Chavez Barajas<sup>58</sup> ,  
M. Chefdeville<sup>10</sup> , C. Chen<sup>12</sup> , S. Chen<sup>5</sup> , Z. Chen<sup>7</sup> , A. Chernov<sup>38</sup> ,  
S. Chernyshenko<sup>50</sup> , V. Chobanova<sup>44,y</sup> , S. Cholak<sup>47</sup> , M. Chrzaszcz<sup>38</sup> , A. Chubykin<sup>41</sup> ,  
V. Chulikov<sup>41</sup> , P. Ciambone<sup>25</sup> , M.F. Cicala<sup>54</sup> , X. Cid Vidal<sup>44</sup> , G. Ciezarek<sup>46</sup> ,  
P. Cifra<sup>46</sup> , P.E.L. Clarke<sup>56</sup> , M. Clemencic<sup>46</sup> , H.V. Cliff<sup>53</sup> , J. Closier<sup>46</sup> ,  
J.L. Cobbledick<sup>60</sup> , C. Cocha Toapaxi<sup>19</sup> , V. Coco<sup>46</sup> , J. Cogan<sup>12</sup> , E. Cogneras<sup>11</sup> ,  
L. Cojocariu<sup>40</sup> , P. Collins<sup>46</sup> , T. Colombo<sup>46</sup> , A. Comerma-Montells<sup>43</sup> , L. Congedo<sup>21</sup> ,  
A. Contu<sup>29</sup> , N. Cooke<sup>57</sup> , I. Corredoira<sup>44</sup> , A. Correia<sup>15</sup> , G. Corti<sup>46</sup> ,  
J.J. Cottee Meldrum<sup>52</sup> , B. Couturier<sup>46</sup> , D.C. Craik<sup>48</sup> , M. Cruz Torres<sup>2,g</sup> , R. Currie<sup>56</sup> ,  
C.L. Da Silva<sup>65</sup> , S. Dadabaev<sup>41</sup> , L. Dai<sup>68</sup> , X. Dai<sup>6</sup> , E. Dall’Occo<sup>17</sup> , J. Dalseno<sup>44</sup> ,  
C. D’Ambrosio<sup>46</sup> , J. Daniel<sup>11</sup> , A. Danilina<sup>41</sup> , P. d’Argent<sup>21</sup> , A. Davidson<sup>54</sup> ,  
J.E. Davies<sup>60</sup> , A. Davis<sup>60</sup> , O. De Aguiar Francisco<sup>60</sup> , C. De Angelis<sup>29,j</sup> ,  
J. de Boer<sup>35</sup> , K. De Bruyn<sup>75</sup> , S. De Capua<sup>60</sup> , M. De Cian<sup>19,46</sup> ,  
U. De Freitas Carneiro Da Graca<sup>2,b</sup> , E. De Lucia<sup>25</sup> , J.M. De Miranda<sup>2</sup> , L. De Paula<sup>3</sup> ,







X. Vilasis-Cardona<sup>42</sup> , E. Vilella Figueras<sup>58</sup> , A. Villa<sup>22</sup> , P. Vincent<sup>15</sup> , F.C. Volle<sup>13</sup> ,  
D. vom Bruch<sup>12</sup> , V. Vorobyev<sup>41</sup> , N. Voropaev<sup>41</sup> , K. Vos<sup>76</sup> , G. Vouters<sup>10</sup> , C. Vrahas<sup>56</sup> ,  
J. Walsh<sup>32</sup> , E.J. Walton<sup>1</sup> , G. Wan<sup>6</sup> , C. Wang<sup>19</sup> , G. Wang<sup>8</sup> , J. Wang<sup>6</sup> ,  
J. Wang<sup>5</sup> , J. Wang<sup>4</sup> , J. Wang<sup>71</sup> , M. Wang<sup>27</sup> , N. W. Wang<sup>7</sup> , R. Wang<sup>52</sup> ,  
X. Wang<sup>69</sup> , X. W. Wang<sup>59</sup> , Y. Wang<sup>8</sup> , Z. Wang<sup>13</sup> , Z. Wang<sup>4</sup> , Z. Wang<sup>7</sup> ,  
J.A. Ward<sup>54,1</sup> , N.K. Watson<sup>51</sup> , D. Websdale<sup>59</sup> , Y. Wei<sup>6</sup> , B.D.C. Westhenry<sup>52</sup> ,  
D.J. White<sup>60</sup> , M. Whitehead<sup>57</sup> , A.R. Wiederhold<sup>54</sup> , D. Wiedner<sup>17</sup> , G. Wilkinson<sup>61</sup> ,  
M.K. Wilkinson<sup>63</sup> , M. Williams<sup>62</sup> , M.R.J. Williams<sup>56</sup> , R. Williams<sup>53</sup> ,  
F.F. Wilson<sup>55</sup> , W. Wislicki<sup>39</sup> , M. Witek<sup>38</sup> , L. Witola<sup>19</sup> , C.P. Wong<sup>65</sup> ,  
G. Wormser<sup>13</sup> , S.A. Wotton<sup>53</sup> , H. Wu<sup>66</sup> , J. Wu<sup>8</sup> , Y. Wu<sup>6</sup> , K. Wyllie<sup>46</sup> , S. Xian<sup>69</sup> ,  
Z. Xiang<sup>5</sup> , Y. Xie<sup>8</sup> , A. Xu<sup>32</sup> , J. Xu<sup>7</sup> , L. Xu<sup>4</sup> , L. Xu<sup>4</sup> , M. Xu<sup>54</sup> , Z. Xu<sup>11</sup> ,  
Z. Xu<sup>7</sup> , Z. Xu<sup>5</sup> , D. Yang<sup>4</sup> , S. Yang<sup>7</sup> , X. Yang<sup>6</sup> , Y. Yang<sup>26,m</sup> , Z. Yang<sup>6</sup> ,  
Z. Yang<sup>64</sup> , V. Yeroshenko<sup>13</sup> , H. Yeung<sup>60</sup> , H. Yin<sup>8</sup> , C. Y. Yu<sup>6</sup> , J. Yu<sup>68</sup> ,  
X. Yuan<sup>5</sup> , E. Zaffaroni<sup>47</sup> , M. Zavertyaev<sup>18</sup> , M. Zdybal<sup>38</sup> , M. Zeng<sup>4</sup> , C. Zhang<sup>6</sup> ,  
D. Zhang<sup>8</sup> , J. Zhang<sup>7</sup> , L. Zhang<sup>4</sup> , S. Zhang<sup>68</sup> , S. Zhang<sup>6</sup> , Y. Zhang<sup>6</sup> , Y. Zhang<sup>61</sup> ,  
Y. Z. Zhang<sup>4</sup> , Y. Zhao<sup>19</sup> , A. Zharkova<sup>41</sup> , A. Zhelezov<sup>19</sup> , X. Z. Zheng<sup>4</sup> ,  
Y. Zheng<sup>7</sup> , T. Zhou<sup>6</sup> , X. Zhou<sup>8</sup> , Y. Zhou<sup>7</sup> , V. Zhovkovska<sup>54</sup> , L. Z. Zhu<sup>7</sup> ,  
X. Zhu<sup>4</sup> , X. Zhu<sup>8</sup> , Z. Zhu<sup>7</sup> , V. Zhukov<sup>16,41</sup> , J. Zhuo<sup>45</sup> , Q. Zou<sup>5,7</sup> , D. Zuliani<sup>30</sup> ,  
G. Zunica<sup>60</sup> .

<sup>1</sup>*School of Physics and Astronomy, Monash University, Melbourne, Australia*

<sup>2</sup>*Centro Brasileiro de Pesquisas Físicas (CBPF), Rio de Janeiro, Brazil*

<sup>3</sup>*Universidade Federal do Rio de Janeiro (UFRJ), Rio de Janeiro, Brazil*

<sup>4</sup>*Center for High Energy Physics, Tsinghua University, Beijing, China*

<sup>5</sup>*Institute Of High Energy Physics (IHEP), Beijing, China*

<sup>6</sup>*School of Physics State Key Laboratory of Nuclear Physics and Technology, Peking University, Beijing, China*

<sup>7</sup>*University of Chinese Academy of Sciences, Beijing, China*

<sup>8</sup>*Institute of Particle Physics, Central China Normal University, Wuhan, Hubei, China*

<sup>9</sup>*Consejo Nacional de Rectores (CONARE), San Jose, Costa Rica*

<sup>10</sup>*Université Savoie Mont Blanc, CNRS, IN2P3-LAPP, Annecy, France*

<sup>11</sup>*Université Clermont Auvergne, CNRS/IN2P3, LPC, Clermont-Ferrand, France*

<sup>12</sup>*Aix Marseille Univ, CNRS/IN2P3, CPPM, Marseille, France*

<sup>13</sup>*Université Paris-Saclay, CNRS/IN2P3, IJCLab, Orsay, France*

<sup>14</sup>*Laboratoire Leprince-Ringuet, CNRS/IN2P3, Ecole Polytechnique, Institut Polytechnique de Paris, Palaiseau, France*

<sup>15</sup>*LPNHE, Sorbonne Université, Paris Diderot Sorbonne Paris Cité, CNRS/IN2P3, Paris, France*

<sup>16</sup>*I. Physikalisches Institut, RWTH Aachen University, Aachen, Germany*

<sup>17</sup>*Fakultät Physik, Technische Universität Dortmund, Dortmund, Germany*

<sup>18</sup>*Max-Planck-Institut für Kernphysik (MPIK), Heidelberg, Germany*

<sup>19</sup>*Physikalisches Institut, Ruprecht-Karls-Universität Heidelberg, Heidelberg, Germany*

<sup>20</sup>*School of Physics, University College Dublin, Dublin, Ireland*

<sup>21</sup>*INFN Sezione di Bari, Bari, Italy*

<sup>22</sup>*INFN Sezione di Bologna, Bologna, Italy*

<sup>23</sup>*INFN Sezione di Ferrara, Ferrara, Italy*

<sup>24</sup>*INFN Sezione di Firenze, Firenze, Italy*

<sup>25</sup>*INFN Laboratori Nazionali di Frascati, Frascati, Italy*

<sup>26</sup>*INFN Sezione di Genova, Genova, Italy*

<sup>27</sup>*INFN Sezione di Milano, Milano, Italy*

<sup>28</sup>*INFN Sezione di Milano-Bicocca, Milano, Italy*

<sup>29</sup>*INFN Sezione di Cagliari, Monserrato, Italy*

<sup>30</sup>*Università degli Studi di Padova, Università e INFN, Padova, Padova, Italy*

<sup>31</sup>*INFN Sezione di Perugia, Perugia, Italy*

<sup>32</sup>*INFN Sezione di Pisa, Pisa, Italy*

- <sup>33</sup> INFN Sezione di Roma La Sapienza, Roma, Italy
- <sup>34</sup> INFN Sezione di Roma Tor Vergata, Roma, Italy
- <sup>35</sup> Nikhef National Institute for Subatomic Physics, Amsterdam, Netherlands
- <sup>36</sup> Nikhef National Institute for Subatomic Physics and VU University Amsterdam, Amsterdam, Netherlands
- <sup>37</sup> AGH - University of Krakow, Faculty of Physics and Applied Computer Science, Kraków, Poland
- <sup>38</sup> Henryk Niewodniczanski Institute of Nuclear Physics Polish Academy of Sciences, Kraków, Poland
- <sup>39</sup> National Center for Nuclear Research (NCBJ), Warsaw, Poland
- <sup>40</sup> Horia Hulubei National Institute of Physics and Nuclear Engineering, Bucharest-Magurele, Romania
- <sup>41</sup> Affiliated with an institute covered by a cooperation agreement with CERN
- <sup>42</sup> DS4DS, La Salle, Universitat Ramon Llull, Barcelona, Spain
- <sup>43</sup> ICCUB, Universitat de Barcelona, Barcelona, Spain
- <sup>44</sup> Instituto Galego de Física de Altas Enerxías (IGFAE), Universidade de Santiago de Compostela, Santiago de Compostela, Spain
- <sup>45</sup> Instituto de Física Corpuscular, Centro Mixto Universidad de Valencia - CSIC, Valencia, Spain
- <sup>46</sup> European Organization for Nuclear Research (CERN), Geneva, Switzerland
- <sup>47</sup> Institute of Physics, Ecole Polytechnique Fédérale de Lausanne (EPFL), Lausanne, Switzerland
- <sup>48</sup> Physik-Institut, Universität Zürich, Zürich, Switzerland
- <sup>49</sup> NSC Kharkiv Institute of Physics and Technology (NSC KIPT), Kharkiv, Ukraine
- <sup>50</sup> Institute for Nuclear Research of the National Academy of Sciences (KINR), Kyiv, Ukraine
- <sup>51</sup> University of Birmingham, Birmingham, United Kingdom
- <sup>52</sup> H.H. Wills Physics Laboratory, University of Bristol, Bristol, United Kingdom
- <sup>53</sup> Cavendish Laboratory, University of Cambridge, Cambridge, United Kingdom
- <sup>54</sup> Department of Physics, University of Warwick, Coventry, United Kingdom
- <sup>55</sup> STFC Rutherford Appleton Laboratory, Didcot, United Kingdom
- <sup>56</sup> School of Physics and Astronomy, University of Edinburgh, Edinburgh, United Kingdom
- <sup>57</sup> School of Physics and Astronomy, University of Glasgow, Glasgow, United Kingdom
- <sup>58</sup> Oliver Lodge Laboratory, University of Liverpool, Liverpool, United Kingdom
- <sup>59</sup> Imperial College London, London, United Kingdom
- <sup>60</sup> Department of Physics and Astronomy, University of Manchester, Manchester, United Kingdom
- <sup>61</sup> Department of Physics, University of Oxford, Oxford, United Kingdom
- <sup>62</sup> Massachusetts Institute of Technology, Cambridge, MA, United States
- <sup>63</sup> University of Cincinnati, Cincinnati, OH, United States
- <sup>64</sup> University of Maryland, College Park, MD, United States
- <sup>65</sup> Los Alamos National Laboratory (LANL), Los Alamos, NM, United States
- <sup>66</sup> Syracuse University, Syracuse, NY, United States
- <sup>67</sup> Pontifícia Universidade Católica do Rio de Janeiro (PUC-Rio), Rio de Janeiro, Brazil, associated to <sup>3</sup>
- <sup>68</sup> School of Physics and Electronics, Hunan University, Changsha City, China, associated to <sup>8</sup>
- <sup>69</sup> Guangdong Provincial Key Laboratory of Nuclear Science, Guangdong-Hong Kong Joint Laboratory of Quantum Matter, Institute of Quantum Matter, South China Normal University, Guangzhou, China, associated to <sup>4</sup>
- <sup>70</sup> Lanzhou University, Lanzhou, China, associated to <sup>5</sup>
- <sup>71</sup> School of Physics and Technology, Wuhan University, Wuhan, China, associated to <sup>4</sup>
- <sup>72</sup> Departamento de Física, Universidad Nacional de Colombia, Bogota, Colombia, associated to <sup>15</sup>
- <sup>73</sup> Universität Bonn - Helmholtz-Institut für Strahlen und Kernphysik, Bonn, Germany, associated to <sup>19</sup>
- <sup>74</sup> Eotvos Lorand University, Budapest, Hungary, associated to <sup>46</sup>
- <sup>75</sup> Van Swinderen Institute, University of Groningen, Groningen, Netherlands, associated to <sup>35</sup>
- <sup>76</sup> Universiteit Maastricht, Maastricht, Netherlands, associated to <sup>35</sup>
- <sup>77</sup> Tadeusz Kosciuszko Cracow University of Technology, Cracow, Poland, associated to <sup>38</sup>
- <sup>78</sup> Department of Physics and Astronomy, Uppsala University, Uppsala, Sweden, associated to <sup>57</sup>
- <sup>79</sup> University of Michigan, Ann Arbor, MI, United States, associated to <sup>66</sup>
- <sup>80</sup> Departement de Physique Nucleaire (SPhN), Gif-Sur-Yvette, France

<sup>a</sup> Universidade de Brasília, Brasília, Brazil

<sup>b</sup> Centro Federal de Educação Tecnológica Celso Suckow da Fonseca, Rio De Janeiro, Brazil

<sup>c</sup> Hangzhou Institute for Advanced Study, UCAS, Hangzhou, China

<sup>d</sup> School of Physics and Electronics, Henan University, Kaifeng, China



- <sup>e</sup> *LIP6, Sorbonne Universite, Paris, France*  
<sup>f</sup> *Excellence Cluster ORIGINS, Munich, Germany*  
<sup>g</sup> *Universidad Nacional Autónoma de Honduras, Tegucigalpa, Honduras*  
<sup>h</sup> *Università di Bari, Bari, Italy*  
<sup>i</sup> *Università di Bologna, Bologna, Italy*  
<sup>j</sup> *Università di Cagliari, Cagliari, Italy*  
<sup>k</sup> *Università di Ferrara, Ferrara, Italy*  
<sup>l</sup> *Università di Firenze, Firenze, Italy*  
<sup>m</sup> *Università di Genova, Genova, Italy*  
<sup>n</sup> *Università degli Studi di Milano, Milano, Italy*  
<sup>o</sup> *Università di Milano Bicocca, Milano, Italy*  
<sup>p</sup> *Università di Padova, Padova, Italy*  
<sup>q</sup> *Università di Perugia, Perugia, Italy*  
<sup>r</sup> *Scuola Normale Superiore, Pisa, Italy*  
<sup>s</sup> *Università di Pisa, Pisa, Italy*  
<sup>t</sup> *Università della Basilicata, Potenza, Italy*  
<sup>u</sup> *Università di Roma Tor Vergata, Roma, Italy*  
<sup>v</sup> *Università di Siena, Siena, Italy*  
<sup>w</sup> *Università di Urbino, Urbino, Italy*  
<sup>x</sup> *Universidad de Alcalá, Alcalá de Henares, Spain*  
<sup>y</sup> *Universidade da Coruña, Coruña, Spain*  
<sup>z</sup> *Department of Physics/Division of Particle Physics, Lund, Sweden*  
<sup>†</sup> *Deceased*